Appendix to Chapter 9

Extreme Sea Level Projections

Authors: Lucy Bricheno[2], Heather Cannaby[2], Tom Howard[1]

Met Office and CSIRO internal reviewers: Kathleen McInnes[3], Matthew Palmer[1]

1 - Met Office, Exeter, UK

2 - National Oceanography Centre, Liverpool, UK

3 - CSIRO, Australia

Contents

Appendix 9.1: Differences in modelled wind field across all GCM and RCM models used.

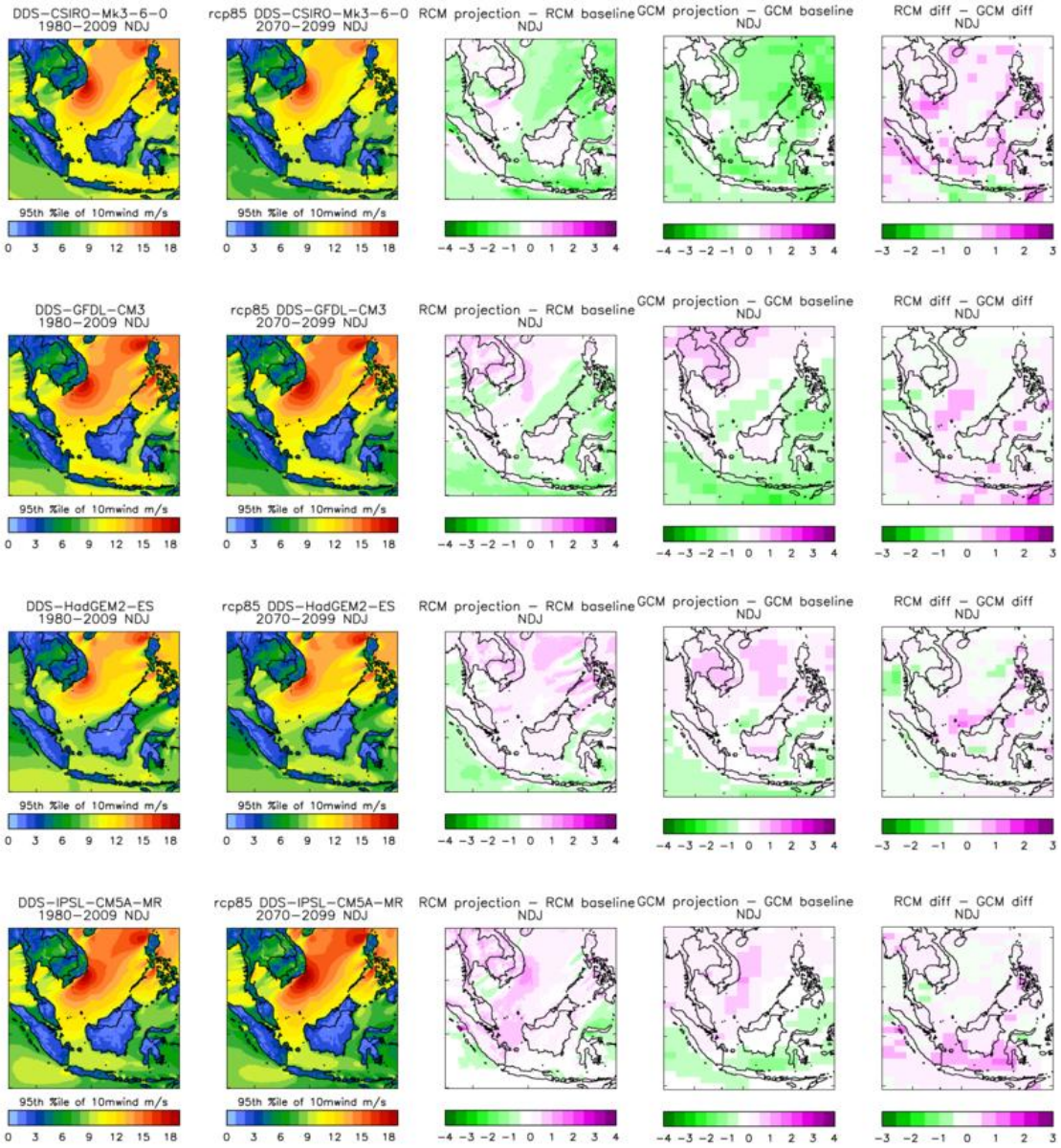

Figure A9.1: 95% percentile (left) and change in 10m wind speed for 9 RCMs (continues on next page)

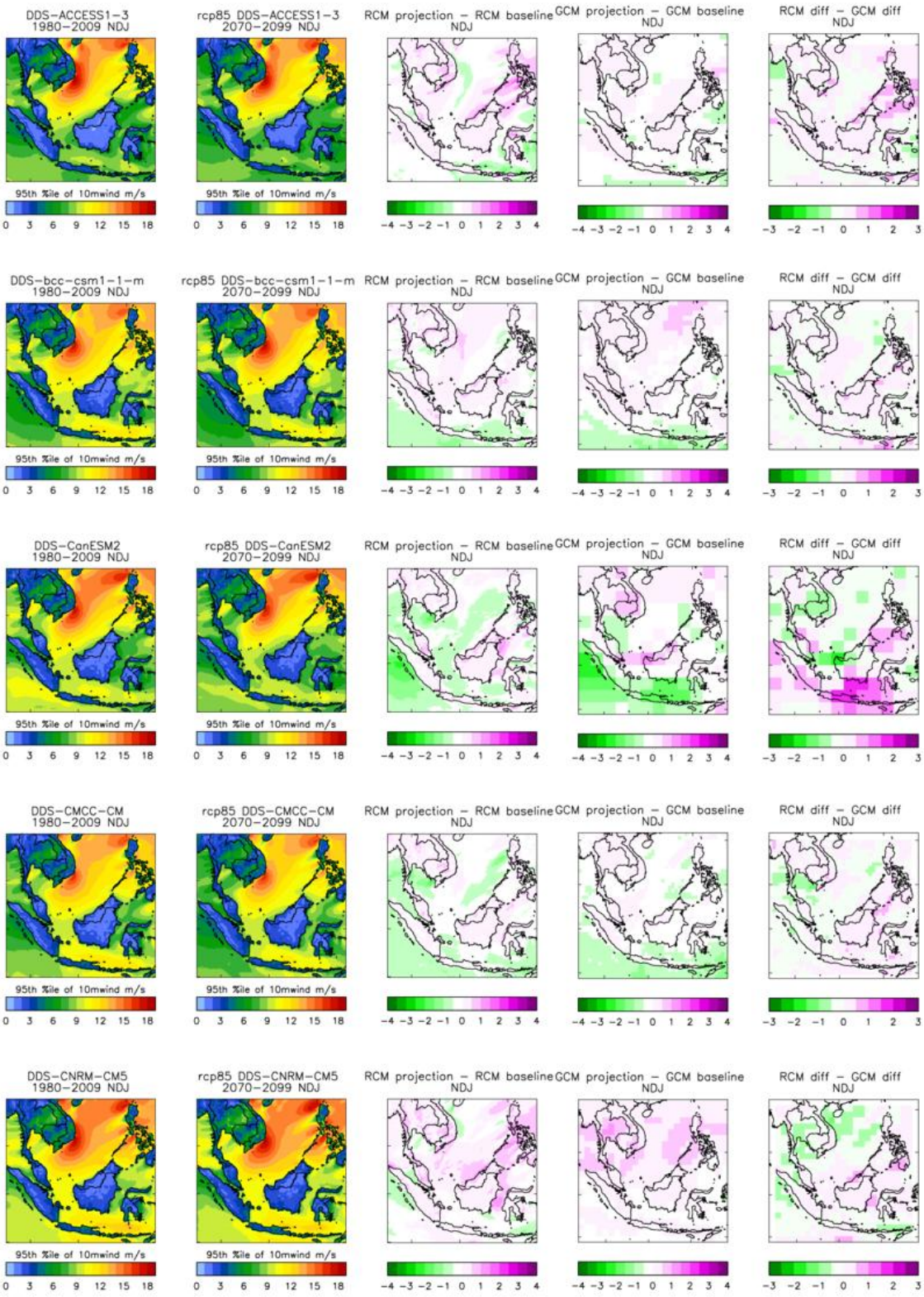
DDS–ACCESS1–3
1980–2009 NDJ
rcp85 DDS–ACCESS1–3
2070–2099 NDJ
RCM projection – RCM baseline
NDJ
GCM projection – GCM baseline
NDJ
RCM diff – GCM diff
NDJ
95th %ile of 10mwind m/s
0 3 6 9 12 15 18
−4 −3 −2 −1 0 1 2 3 4
−3 −2 −1 0 1 2 3
DDS–bcc–csm1–1–m
1980–2009 NDJ
rcp85 DDS–bcc–csm1–1–m
2070–2099 NDJ
DDS–CanESM2
1980–2009 NDJ
rcp85 DDS–CanESM2
2070–2099 NDJ
DDS–CMCC–CM
1980–2009 NDJ
rcp85 DDS–CMCC–CM
2070–2099 NDJ
DDS–CNRM–CM5
1980–2009 NDJ
rcp85 DDS–CNRM–CM5
2070–2099 NDJ

Appendix 9.2: Skew-surge metric

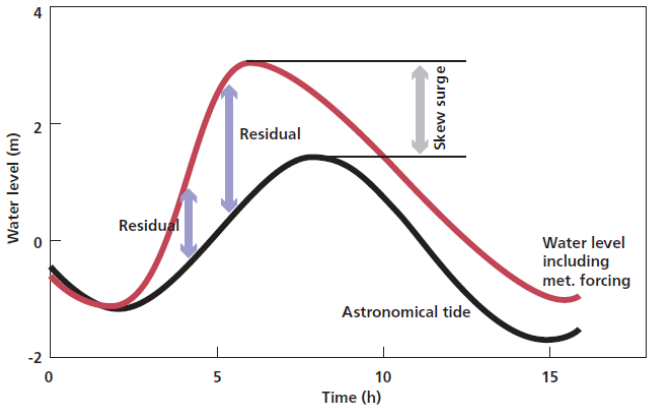

Figure A9.2: Schematic diagram showing how skew surge and surge residual are evaluated. The surge residual evolves throughout the tidal cycle, typically peaking before the astronomical or meteorologically forced tide, whereas the skew surge is evaluated once and is a more useful measure.

Appendix 9.3: Methodology for CMIP5 WaveWatch III simulations

An number of CMIP5 models were used to drive a global wave model WaveWatchIII (WW3). Here we give a brief overview of the methodology used.
WaveWatchIII (Tolman 2009) is a third generation wave model developed by NOAA/NCEP. We used version 3.14 with Tolman and Chalikov (1996) physics. Other changes from the default model settings include the source terms: STABSH=1.4, SWELLF=0.12, and the use of a 2nd order UNO propagation scheme (default is 3rd order). The model is forced with 10m winds (both U and V components) and sea ice.

Experimental design

6 CMIP 5 models (**Table A9.1**) were selected based on their ability to replicate important features of the SE Asian climate and data availability. For each model, the historical scenario, as well as rcp4.5 and rcp8.5 were simulated, with the RCP runs spun off the historic run. Additionally, a simulation forced by ERA Interim data was undertaken for validation purposes.

Table A9.1: Model Simulations

	Historic (1950-2005)	**rcp4.5 (2006-2100)**	**rcp8.5 (2006-2100)**	**Calendar**
ERAI	Yes	No	No	Gregorian
CNRM-CM5-CM5	Yes	Yes	Yes	360 day
GFDL-CM3-CM3	Yes	Yes	Yes	no leap
GFDL-CM3-ESM2G	Yes	Yes	Yes	no leap
GFDL-CM3-ESM2M	Yes	Yes	Yes	no leap
HadGEM2-ES	Yes	Yes	Yes	360 day
IPSL-CM5A-MR	Yes	Yes	Yes	Gregorian

Three different calendars were used between the different simulations: Gregorian; 360 day; and no leap. Different pre-processing routines and different compiled versions of WW3 were needed for each calendar.
The model was forced with 3 hourly wind (*uas* and *vas*) and daily sea ice (*sic*) values taken from the CMIP5 models. These were interpolated onto the WW3 model domain.
Three-hourly wind data was not available for the entire future period for IPSL-CM5A-MR_CM5A_MR, and so daily data were used (2046-2065).

Model Domain

WW3 was set up for a global domain, with a Spherical Multiple Cell (SMC) grid. This is a regular lat-long, with an increased longitudinal poleward of 60° and 74° latitude . The model resolution is 0.7031250° x 0.4687500°, and extends to ~80°N/S

Model output

Model fields were saved every 3 hour for a range of model diagnostics (see **Table A9.2**), and these were used to calculated monthly mean values (both of which were archived). To allow regional downscaling, the model produced nest files for two regional domains, centred on Singapore, and on the UK.

Table A9.2 Model diagnostics

Model diagnostics
Eastward wind
Northward wind
Significant wave height
Wave mean direction
Wave peak frequency
Sea ice area fraction
Sub range wave height band 1
Sub range wave height band 2
Sub range wave height band 3
Sub range wave height band 4
Mean wave period Tm01

Appendix 9.4: Comparison of wave models forced by 4 different RCMs

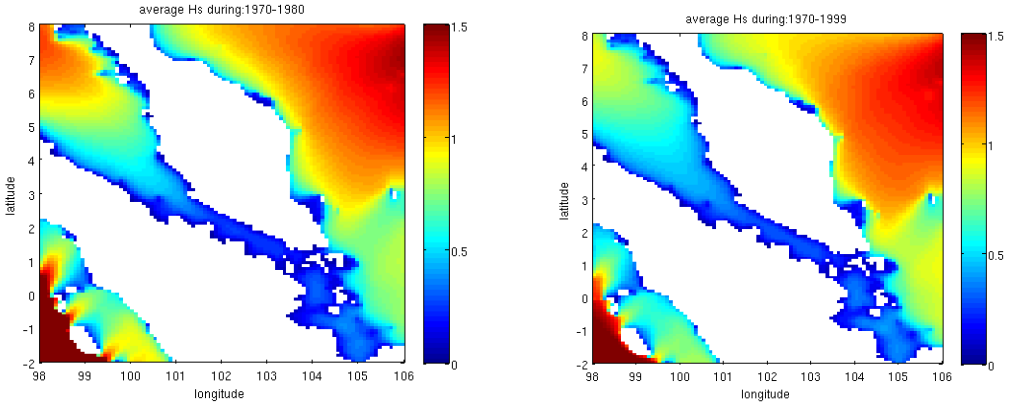

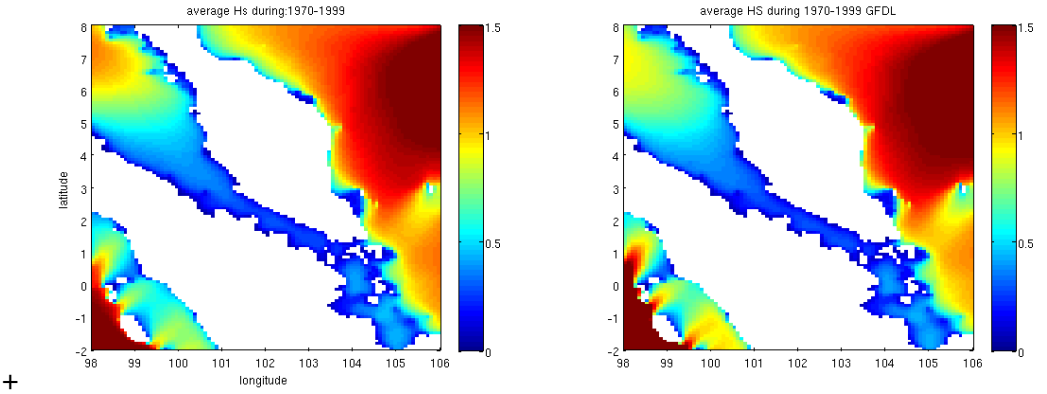

+

Figure A9.3: Average Hs (a) HadGEM2-ES (b) CNRM-CM5 (c) IPSL-CM5A-MR (d) GFDL-CM3-CM3

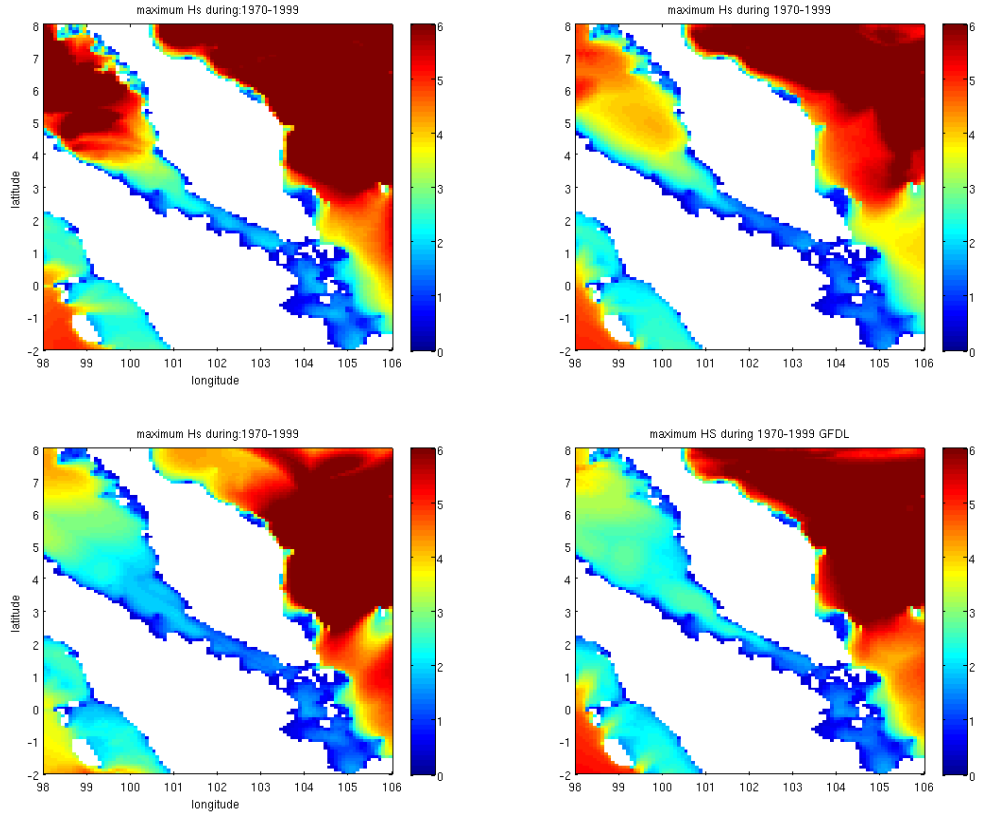

Figure A9.4: Maximum Hs (a) HadGEM2-ES (b) CNRM-CM5 (c) IPSL-CM5A-MR (d) GFDL-CM3-CM3 over a 30 year period (historic).

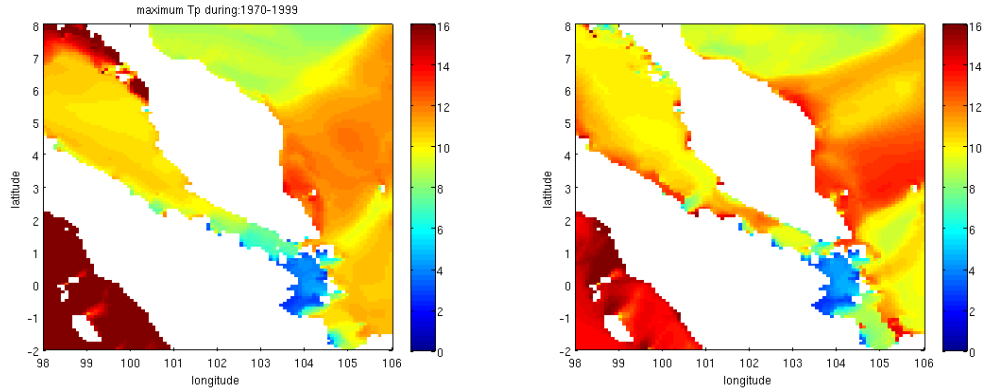

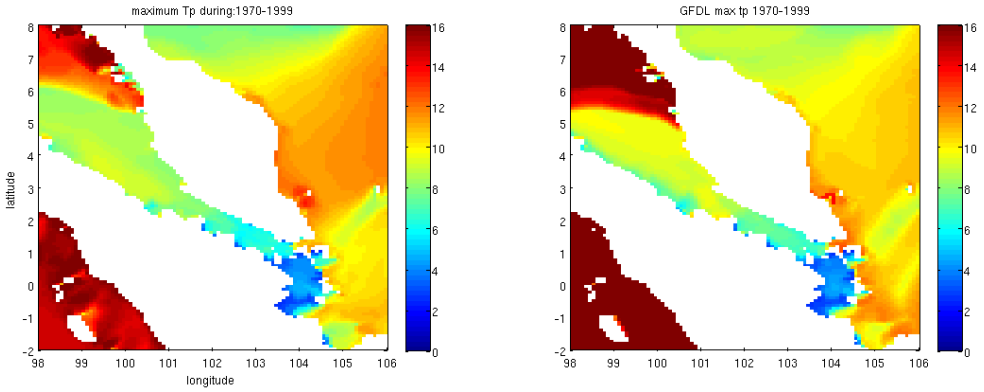

Figure A9.5: Maximum peak wave period (a) HadGEM-ES (b) CNRM-CM5 (c) IPSL-CM5A-MR (d) GFDL-CM3-CM3 over a 30 year period (historic).

Appendix 9.5 Land-Sea breezes

A strong daily cycle is noted in some points close to Singapore. This is believed to be caused by land-sea breezes. Looking a series of points becoming increasingly 'offshore' as the numbers ascend going from West to East (1= red, 2= pink, 3= blue, 4= black), we can see that the small near-shore waves affected by the daily cycle give way to larger swell waves approaching from the South China Sea.

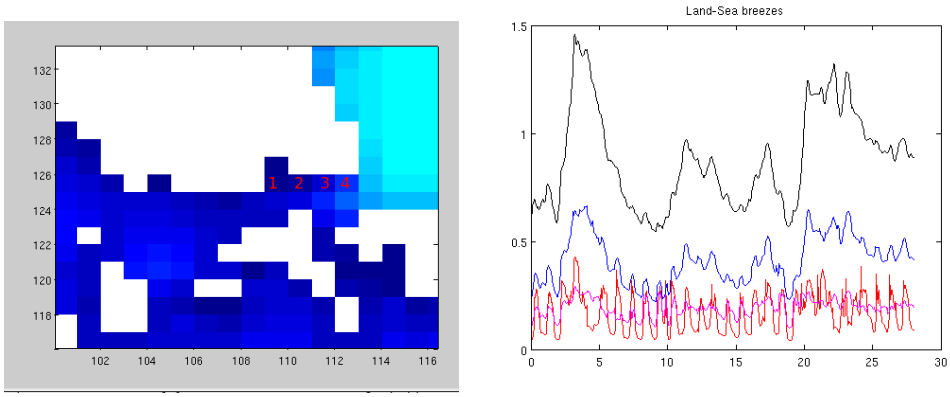

Figure A9.6: Locations and time series representing land-sea breezes

Appendix 9.6 Standard diagnostic plots for stationary fit to skew surge annual maxima from CNRM-CM5, GFDL-CM3 and IPSL-CM5A-MR simulations

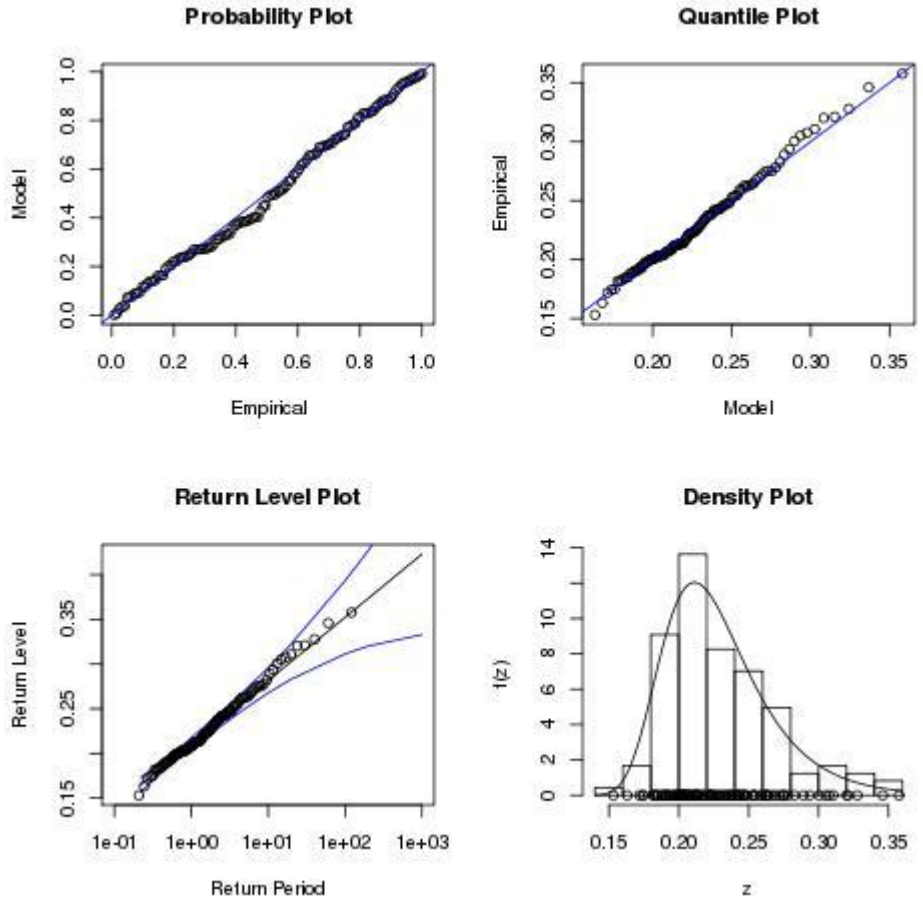

Figure A9.7: Standard diagnostic plots for a stationary GEV fit to the annual maximum skew surges from the CNRM-CM5 simulation.

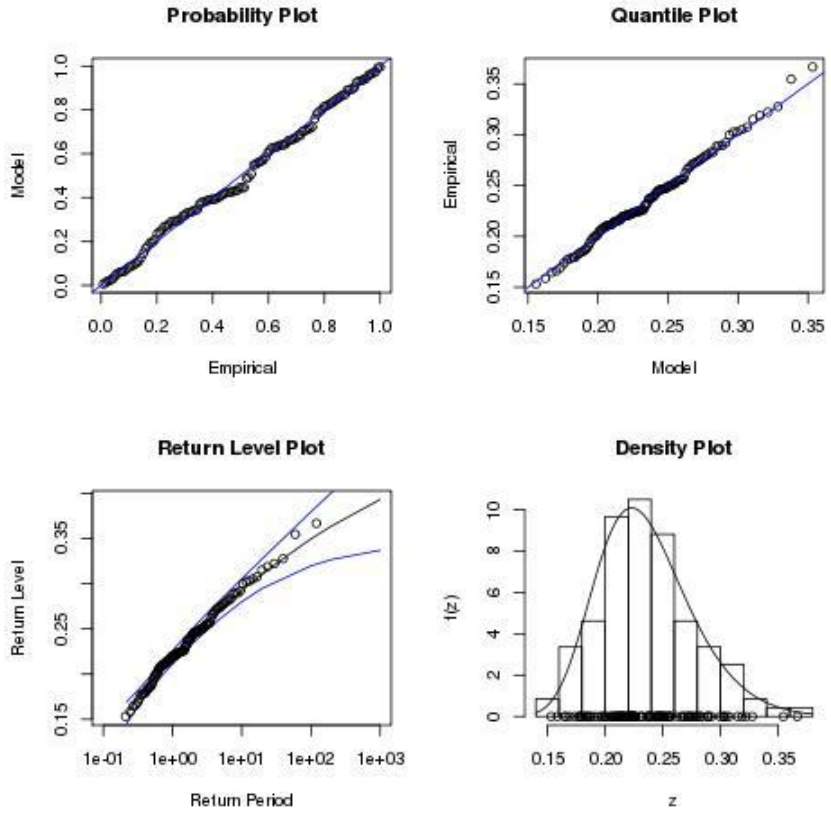

Figure A9.8: Standard diagnostic plots for a stationary GEV fit to the annual maximum skew surges from the GFDL-CM3 simulation.

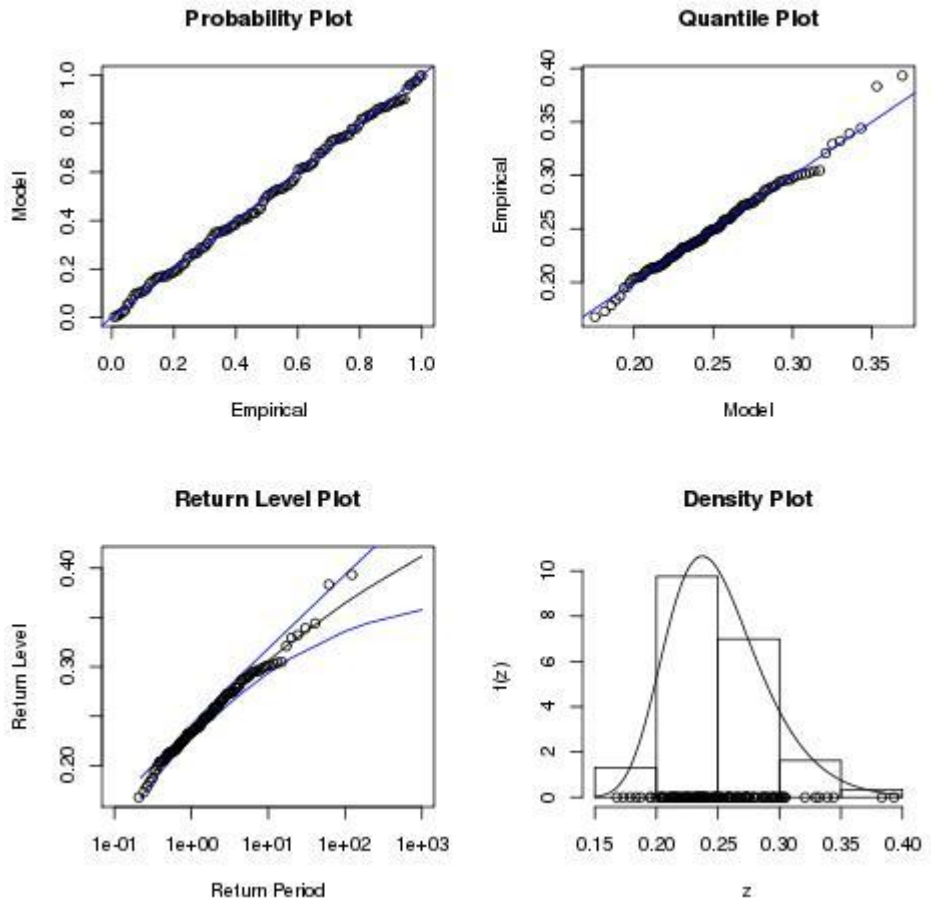

Figure A9.9: Standard diagnostic plots for a stationary GEV fit to the annual maximum skew surges from the IPSL-CM5A-MR simulation.

Appendix 9.7: Further wave model results

Return level and diagnostic plots for stationary GEV fit to extreme significant wave height events

Given the absence of any statistically significant century-scale trends in the extremes of significant wave height in the GFDL-CM3 and HadGEM2-ES simulations, it is legitimate to use a stationary GEV fit to all of the available data, in order to produce a return level plot of significant wave height for each of these two models. Return level plots for a location close to Singapore (site c, see Figure 9.12), along with standard diagnostic plots, are shown in the following figures. Incidentally, the empirical return period of the largest event in a 130-year time series is 130 years, which means that the largest event often looks like an 'outlier' on the return level plot. This illustrates the value of fitting an extreme value model such as the GEV to give a more robust estimate of the long-period return levels.

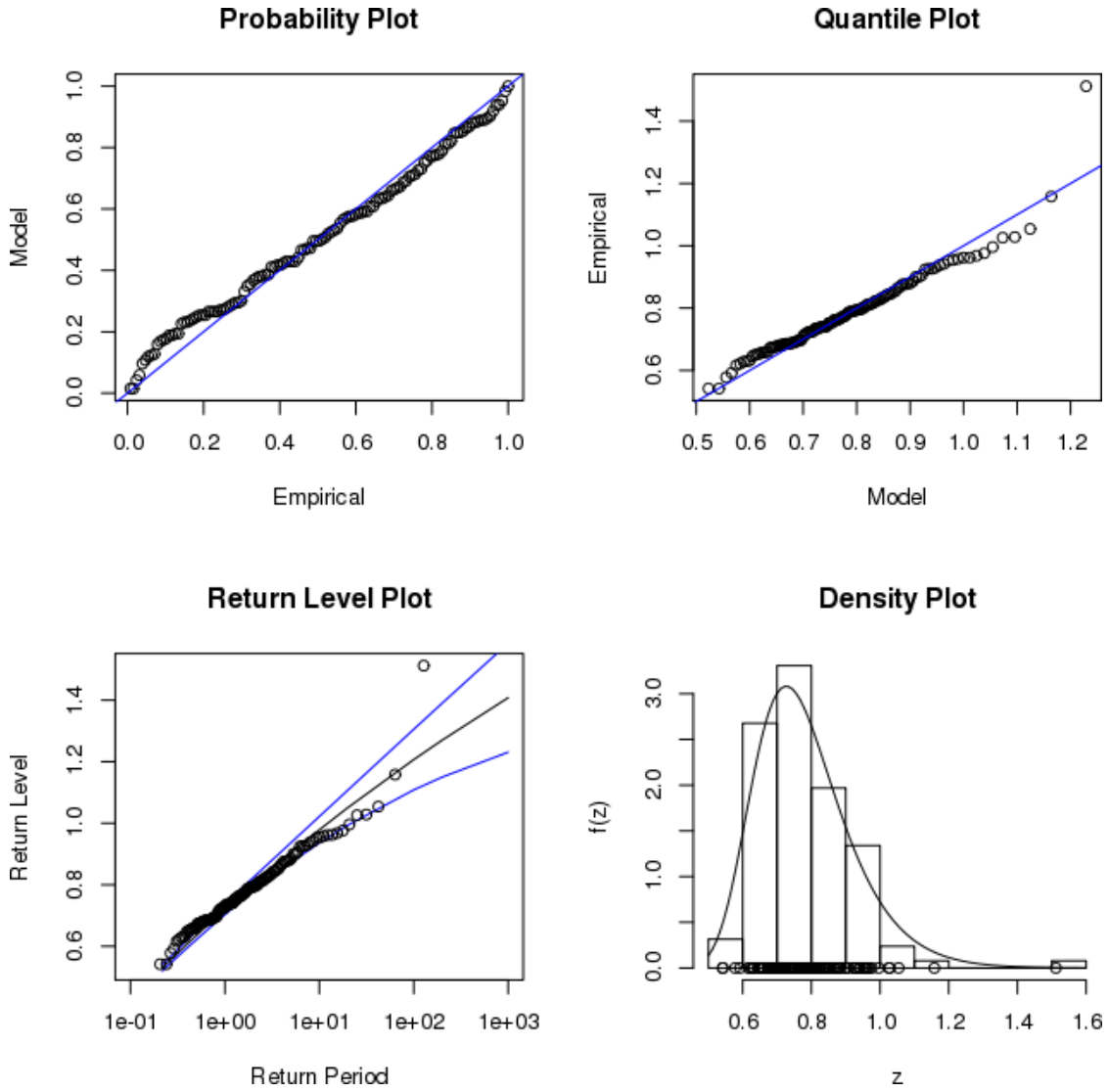

Figure A9.10: Return level and diagnostic plots for HadGEM2-ES close to Singapore (site c) with a stationary fit to all of the available of data.

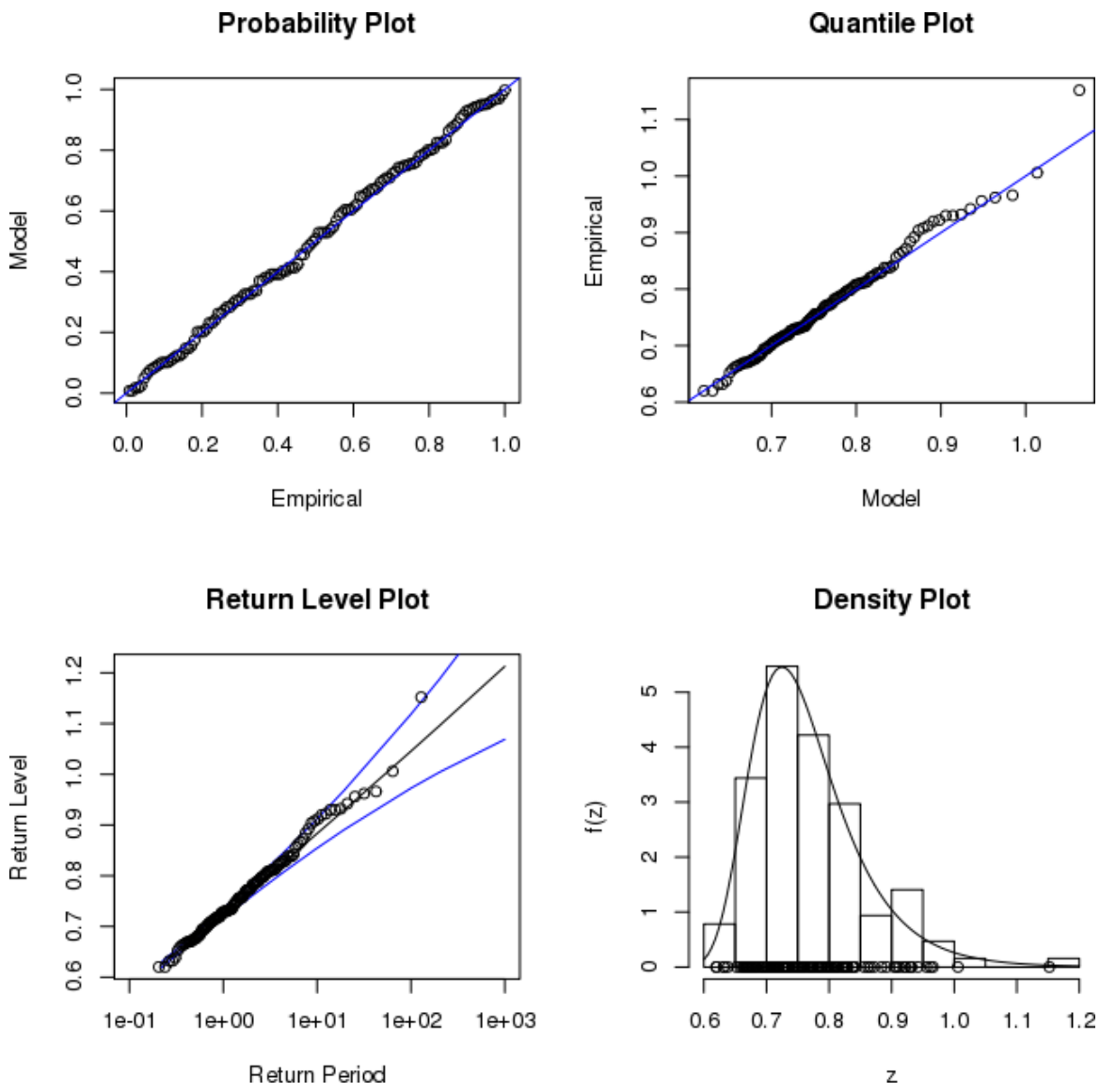

Figure A9.11: Return level and diagnostic plots for GFDL-CM3 close to Singapore (site c) with a stationary fit to all of the available data

Appendix 9.8: Spatial correlation of tide and surge in the NEMO model around the island of Singapore.

In this appendix we present further evidence in support of our approach of analyzing century-scale change in extreme surge at one representative grid point. First we consider a short sample time series from one of the simulations to give an indication of the level of variation between grid points. The time series is shown in Figure A9.12. We have emphasized grid point a, which has the largest signal and grid point j, which has the smallest (see Figure 9.12 for location of the gridpoints). The strong similarity in the time series at the 13 grid points is apparent.

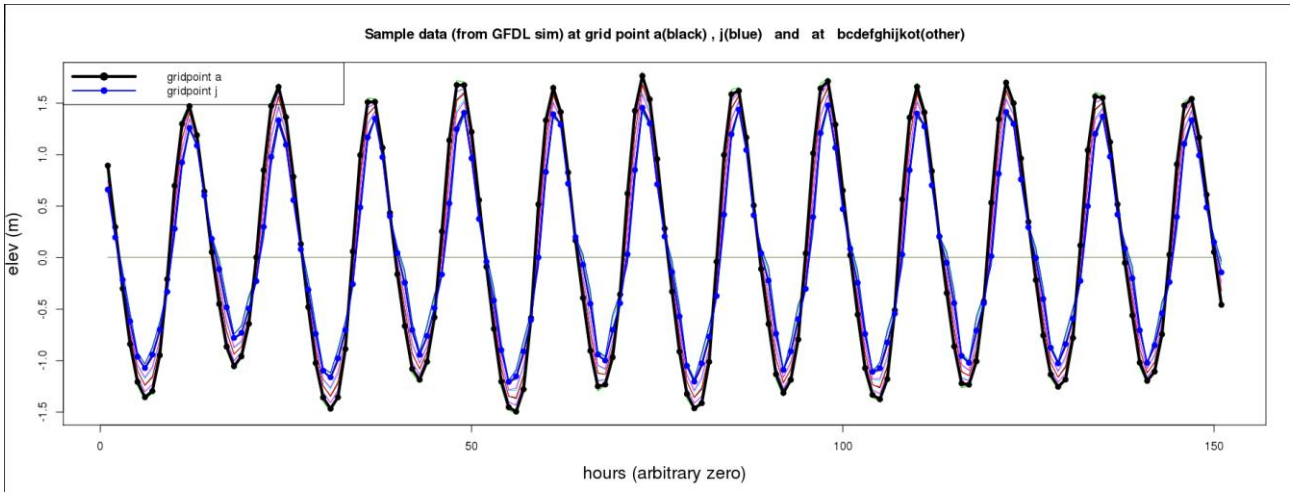

Figure A9.12: Sample time series from one model simulation for all of the 13 active grid points around Singapore (see Figure 9.12). Grid point a, which has the largest signal (during this sample) is shown in black. Grid point j, which has the smallest signal (during this sample) is shown in blue. The thin coloured lines show the other eleven grid points; it can be seen that during this sample these lie between the signal at a and the signal at j.

An alternative view of spatial variations is presented in **Figure A9.13**. This shows a transect of sea surface elevation (with latitude fixed) through grid points abcde and extending over much more of the domain to cover a distance of the order of the size of a tide, at several different times. It can be seen that abcde move almost in phase, illustrating that Singapore is small compared to a (modelled) tidal oscillation.

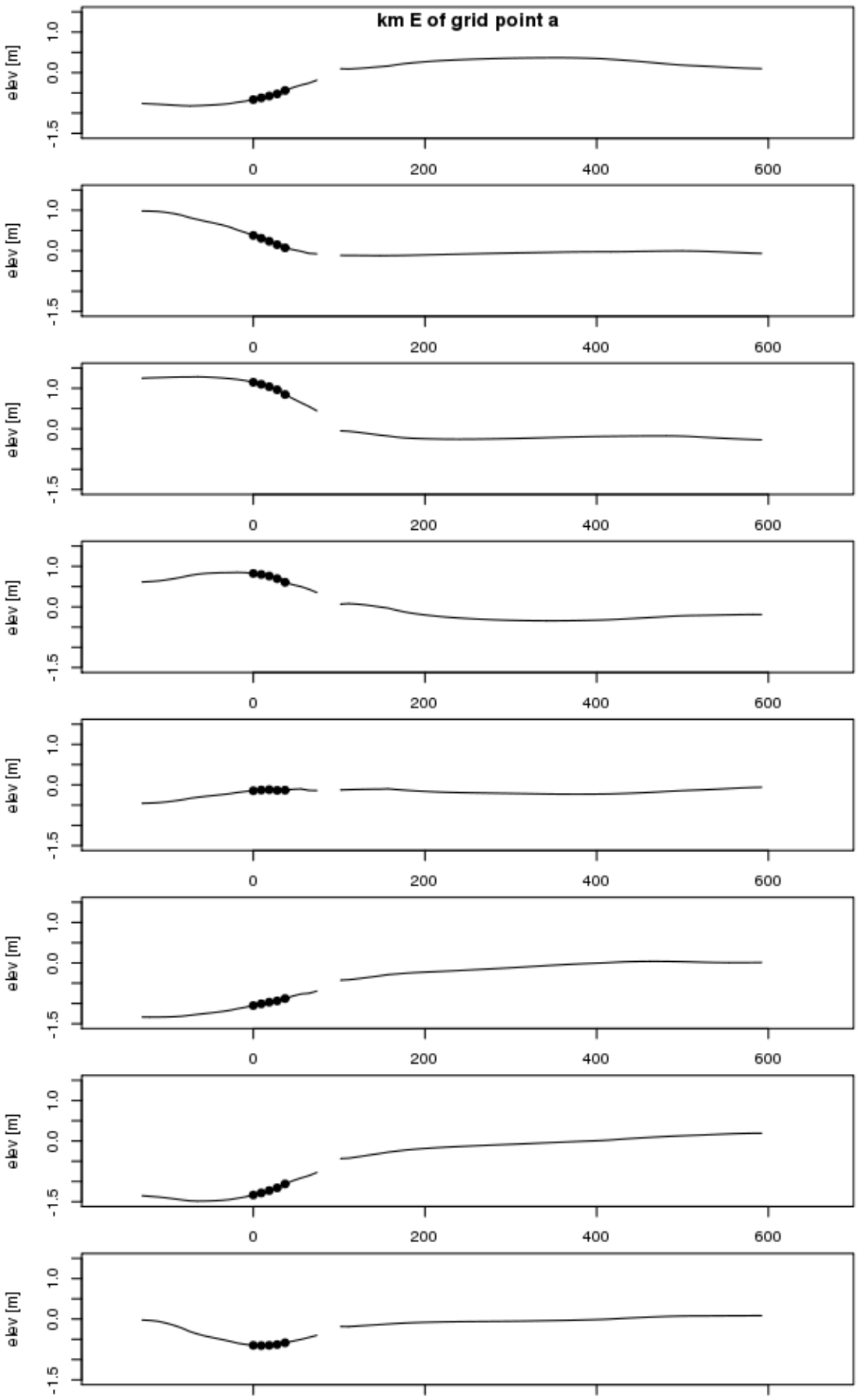

Figure A9.13: Grid points abcde seen in the context of a tidal oscillation. The x-axis shows kilometers east of grid point a. The y-axis shows elevation in metres. Panels show different times in the tidal cycle; from top to bottom: (0, 4, 6, 8, 10, 12, 14, 16) hours from an arbitrary zero. Elevations at grid points abcde are shown by the filled circles. For full details see main text.

Finally we present modelled extremes of skew surge. Figure A9.14 shows a scatter plot of annual max skew surge at pixel t vs pixel a for all years and all models. It is apparent that the extreme events at the two locations are strongly correlated (Pearson's R=0.82).

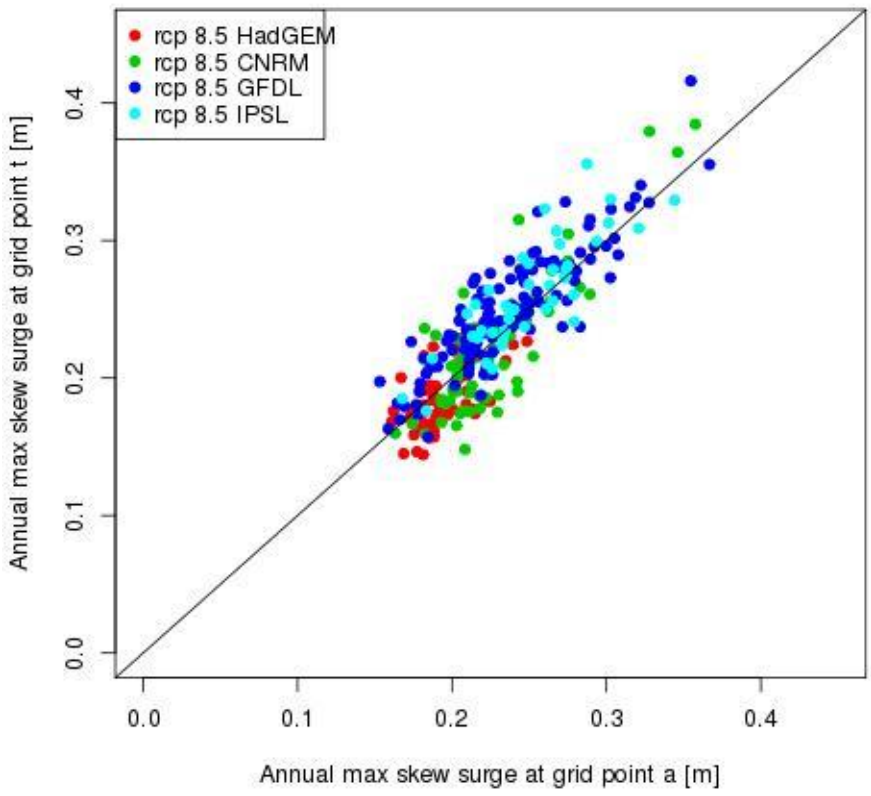

Figure A9.14: Annual maximum skew surge at grid point t (y axis) vs. Grid point a (x axis) for all years of the simulation and all models. The line shows y=x.

In summary:

1) Modeled sea levels at all 13 model grid points around Singapore are strongly correlated.

2) The tidal signal at grid point a is slightly larger than at any of the other 12 grid points, at least for the sample considered here.

3) Annual max skew at grid point t (NW corner) is strongly correlated with that at grid point a (SE corner), which suggests that the (absence of) century-scale change will be similar at all 13 grid points.

Appendix 9.9: Example projected future extreme still water levels.

Following the example calculations of section 9.4.2 we here present projected changes in extreme still water level and example projected future extreme still water levels under RCP8.5 and RCP4.5, for 3 future periods of interest.

Following the example calculations shown in section 9.4.1 we obtain projected changes in extreme sea levels as follows:

Table A9.3: Projected Change in extreme still water level due to changes in regional mean sea level and changes in atmospheric storminess (metres).

2040 RCP8.5					
Period(years)	2	20	100	1000	10000
Lower	0.11	0.11	0.10	0.10	0.09
Centr	0.18	0.18	0.18	0.17	0.17
Upper	0.24	0.23	0.24	0.24	0.25
2070 RCP8.5					
Period(years)	2	20	100	1000	10000
Lower	0.26	0.25	0.24	0.22	0.20
Centr	0.41	0.40	0.40	0.40	0.40
Upper	0.56	0.56	0.57	0.58	0.59
2100 RCP8.5					
Period(years)	2	20	100	1000	10000
Lower	0.44	0.43	0.41	0.38	0.36
Centr	0.73	0.72	0.72	0.71	0.71
Upper	1.04	1.03	1.05	1.06	1.07
2040 RCP4.5					
Period(years)	2	20	100	1000	10000
Lower	0.10	0.10	0.10	0.09	0.08
Centr	0.17	0.17	0.17	0.16	0.16
Upper	0.23	0.22	0.23	0.23	0.24
2070 RCP4.5					
Period(years)	2	20	100	1000	10000
Lower	0.19	0.18	0.17	0.16	0.15
Centr	0.34	0.33	0.33	0.33	0.33
Upper	0.47	0.47	0.47	0.48	0.49
2100 RCP4.5					
Period(years)	2	20	100	1000	10000
Lower	0.28	0.27	0.25	0.23	0.22
Centr	0.51	0.50	0.50	0.50	0.49
Upper	0.74	0.74	0.75	0.76	0.77

Next, illustrative projected future extreme still water levels are formed by combining the above changes linearly with the following example present-day return levels at a particular tide gauge location:

Table A9.4: Illustrative present-day return levels.

Period (years)	2	20	100	1000	10000
Level (metres)	1.79	2.15	2.39	2.75	3.10

Please note that these values are arbitrary and used for illustration only. Please note also that these present-day estimates do not include any uncertainty bounds. In practice it is likely that uncertainties in the present-day levels will form a significant part of the overall uncertainty in projections of future return levels.

Table A9.5: Example projected future extreme still water levels at a tide gauge location (based on the arbitrary illustrative present-day levels shown above in Table A9.4), including changes in regional mean sea level and changes in atmospheric storminess (metres).

2040 RCP8.5					
Period(years)	2	20	100	1000	10000
Lower	1.91	2.26	2.49	2.85	3.19
Centr	1.97	2.32	2.57	2.92	3.27
Upper	2.03	2.38	2.63	2.99	3.35
2070 RCP8.5					
Period(years)	2	20	100	1000	10000
Lower	2.05	2.39	2.63	2.97	3.30
Centr	2.20	2.55	2.79	3.15	3.50
Upper	2.35	2.71	2.96	3.33	3.69
2100 RCP8.5					
Period(years)	2	20	100	1000	10000
Lower	2.23	2.57	2.80	3.13	3.46
Centr	2.52	2.87	3.11	3.46	3.81
Upper	2.83	3.18	3.44	3.81	4.17
2040 RCP4.5					
Period(years)	2	20	100	1000	10000
Lower	1.90	2.25	2.49	2.84	3.18
Centr	1.96	2.31	2.56	2.91	3.26
Upper	2.02	2.37	2.62	2.98	3.34
2070 RCP4.5					
Period(years)	2	20	100	1000	10000
Lower	1.98	2.33	2.56	2.91	3.25
Centr	2.13	2.48	2.72	3.08	3.43
Upper	2.26	2.61	2.86	3.23	3.59
2100 RCP4.5					
Period(years)	2	20	100	1000	10000
Lower	2.07	2.41	2.64	2.98	3.32
Centr	2.30	2.65	2.89	3.25	3.59
Upper	2.53	2.89	3.14	3.51	3.87

Appendix 9.10 Further Tide-Surge Model Validation

Here we compare model simulations of extreme water level with tide-gauge records. We compare simulated annual maximum extreme water levels at grid point 'a' (see chapter 9 figure 9.12) with tide-gaude records at Raffles Light House. Available records cover the years 1996-2013 inclusive – an eighteen-year period. In order to make a like-for-like comparison we extract six non-overlapping samples of eighteen consecutive years from each of the model simulations. To compensate for the different zero offsets (tide-gauge data usually use a zero of the lowest astronomical tide, whereas the model uses a zero of the undisturbed water level), in each case we subtract the eighteen-year mean water level. Then we find the eighteen annual maxima. These data are plotted in figure A9.15.

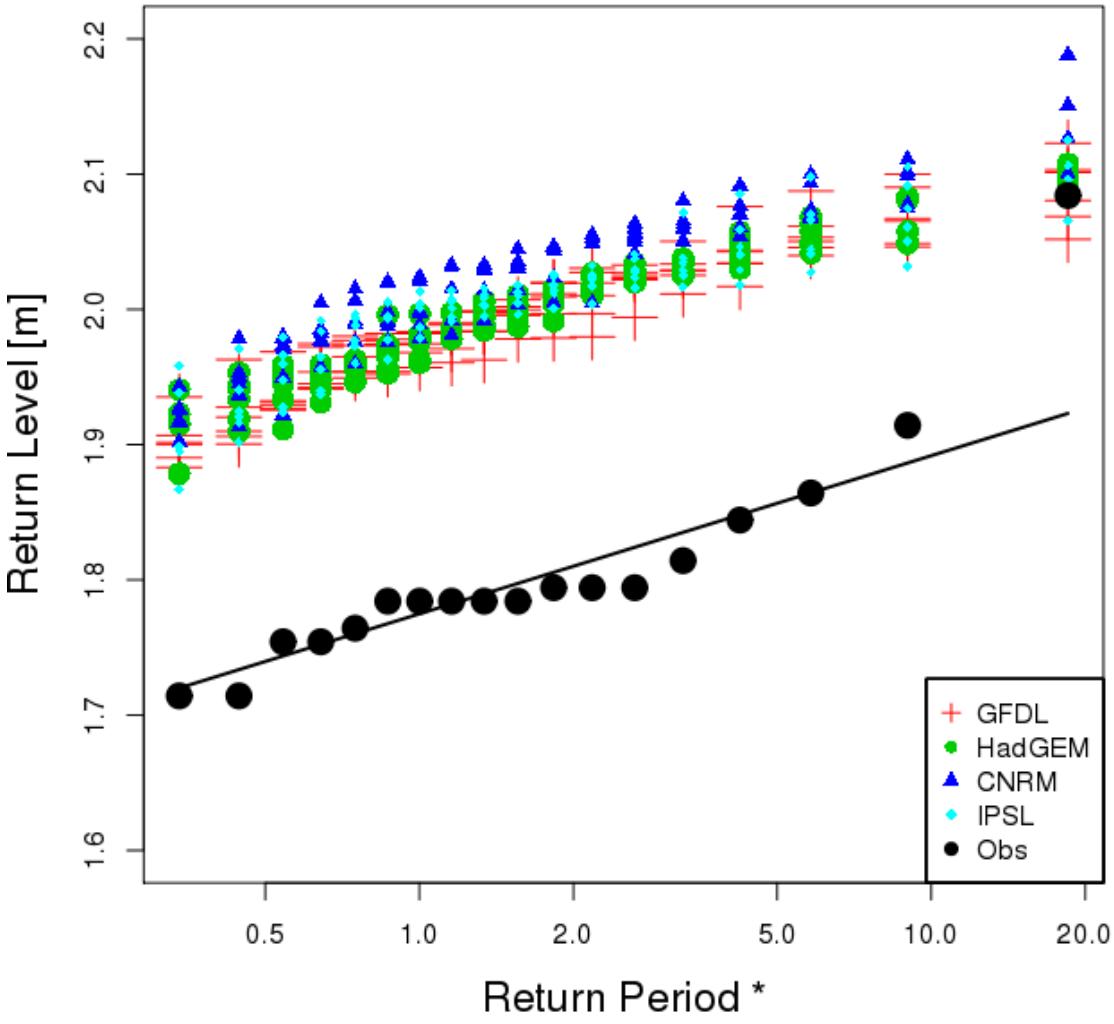

Figure A9.15: Empirical return level data of extreme water level based on 18 years of data from Raffles Light House tide gauge (Obs) and 18-year long samples from the model simulations, at grid point 'a'. The fitted Gumbel distribution of the observations is shown by the straight line. Return Period*: see main text.

We follow the usual convention of plotting the return level against a modified return period RP^* defined by

$$RP^* = \frac{1}{log\left(\frac{RP}{RP-1}\right)}$$

where RP is the return period defined by $RP = 1/prob$(exceedance in any one year).

RP^* is very close to RP for large return periods. The advantage of using RP^* is that a Gumbel distribution appears as a straight line on the return level plot, even for small return periods.

From figure A9.15 we can see that the location parameter of the modelled extreme water levels is larger than that of the observations (i.e. the model data is offset up the Y axis compared to the observations); this is related to the fact that the simulated tidal range at grid point 'a' is larger than the observed tidal range at Raffles Light House. More importantly, what can also be seen is that the scale parameter (the 'gradient' seen in figure A9.15) of the model data is comparable to that of the observations. This is important because it tells us that the model is doing a good job of simulating the inter-annual variability (or 'spread') in extreme water levels. The scale parameter measures this spread.

We have fitted a Gumbel distribution to the tide-gauge observations as shown by the straight line in figure A9.15. We also fitted a Gumbel distribution to each of the samples of model data, to give a distribution of model scale parameters. This distribution, along with the scale parameter of the observations, is shown in figure A9.16. It can be seen that the scale parameter of the observations lies comfortably within the distribution from the model samples. Detrending observed and model data has little effect on this result.

In conclusion, this shows that the observed scale parameter is well modelled. This is important because (outside of the mean sea-level uncertainty) it is the uncertainty in the scale parameter that primarily determines the uncertainty in long-period return levels (i.e. the uncertainty in the most extreme events). Thus good agreement between the modelled and observed scale parameter increases our confidence in the applying the modelled century-scale changes in the most extreme events to present-day tide-gauge data, to produce site-specific projections.

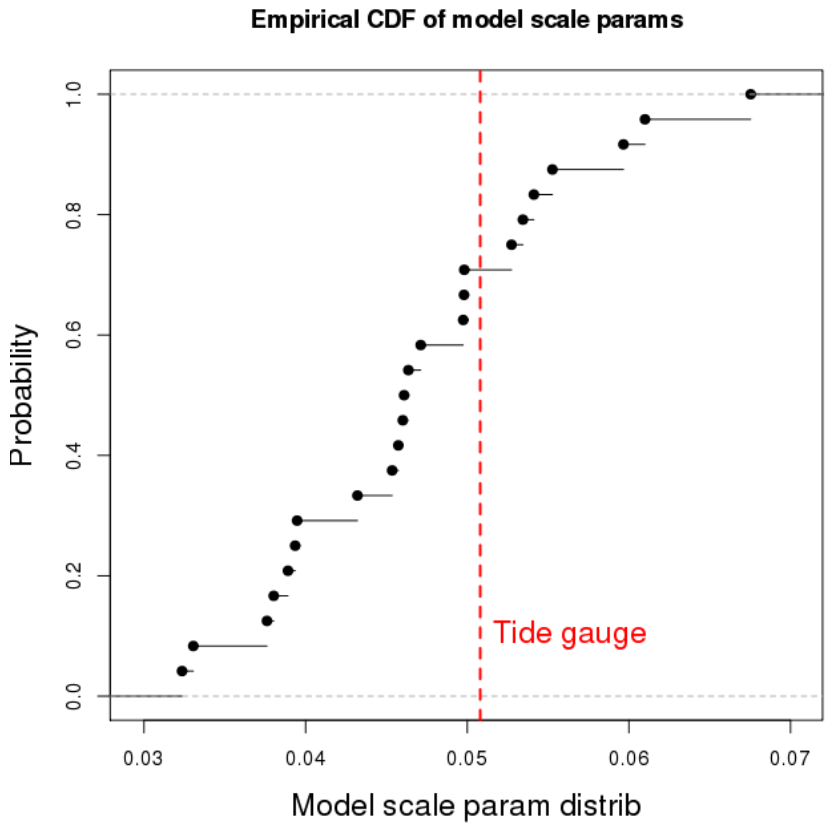

Figure A9.16: Empirical cumulative density function of the scale parameters of the model samples, showing that the scale parameter of the tide gauge data sits well within the model distribution.